Satb1 regulates the self-renewal of hematopoietic stem cells by promoting quiescence and repressing differentiation commitment

Britta Will[1,2], Thomas O Vogler[1], Boris Bartholdy[1], Francine Garrett-Bakelman[3], Jillian Mayer[1], Laura Barreyro[1], Ashley Pandolfi[1], Tihomira I Todorova[1], Ujunwa C Okoye-Okafor[1], Robert F Stanley[1], Tushar D Bhagat[4], Amit Verma[2,4–6], Maria E Figueroa[7], Ari Melnick[3], Michael Roth[1] & Ulrich Steidl[1,2,5,6]

How hematopoietic stem cells (HSCs) coordinate the regulation of opposing cellular mechanisms such as self-renewal and differentiation commitment remains unclear. Here we identified the transcription factor and chromatin remodeler Satb1 as a critical regulator of HSC fate. HSCs lacking *Satb1* had defective self-renewal, were less quiescent and showed accelerated lineage commitment, which resulted in progressive depletion of functional HSCs. The enhanced commitment was caused by less symmetric self-renewal and more symmetric differentiation divisions of Satb1-deficient HSCs. Satb1 simultaneously repressed sets of genes encoding molecules involved in HSC activation and cellular polarity, including *Numb* and *Myc*, which encode two key factors for the specification of stem-cell fate. Thus, Satb1 is a regulator that promotes HSC quiescence and represses lineage commitment.

In metazoans, adult tissue-specific stem cells constitute a rare population of long-lived cells with the ability to give rise to many differentiated cell types. Hematopoietic stem cells (HSCs) ensure the life-long generation of all cells of the innate and adaptive immune systems, as well as red blood cells and platelets[1]. Like many other tissue-specific stem cells in multicellular organisms, HSCs have key features that separate them functionally from differentiated cell types, including relative cellular quiescence, self-maintenance and multilineage differentiation ability[2,3]. Balancing the self-renewal and differentiation of HSCs is crucial for long-term maintenance of the pool of functional HSCs and thus for their ability to sustain blood-cell production and regeneration[4]. Alterations in the balance of quiescence and activation, self-renewal and differentiation are known to exhaust HSCs[5] or lead to their malignant transformation[6].

Transcriptional regulation by specific factors is critical for ensuring the appropriate function of both embryonic and adult tissue-specific stem cells, in part by governing their ability to self-renew and differentiate[7]. The interaction of transcriptional programs, rather than the individual transcription factors themselves, determines the entire set of stem-cell functions, including fate 'decisions'[8,9]. However, how individual functions such as stem-cell quiescence, division and lineage commitment are coordinately regulated is only beginning to be understood. Global epigenetic regulation has been shown to have an important role in the function and lineage differentiation of stem cells,
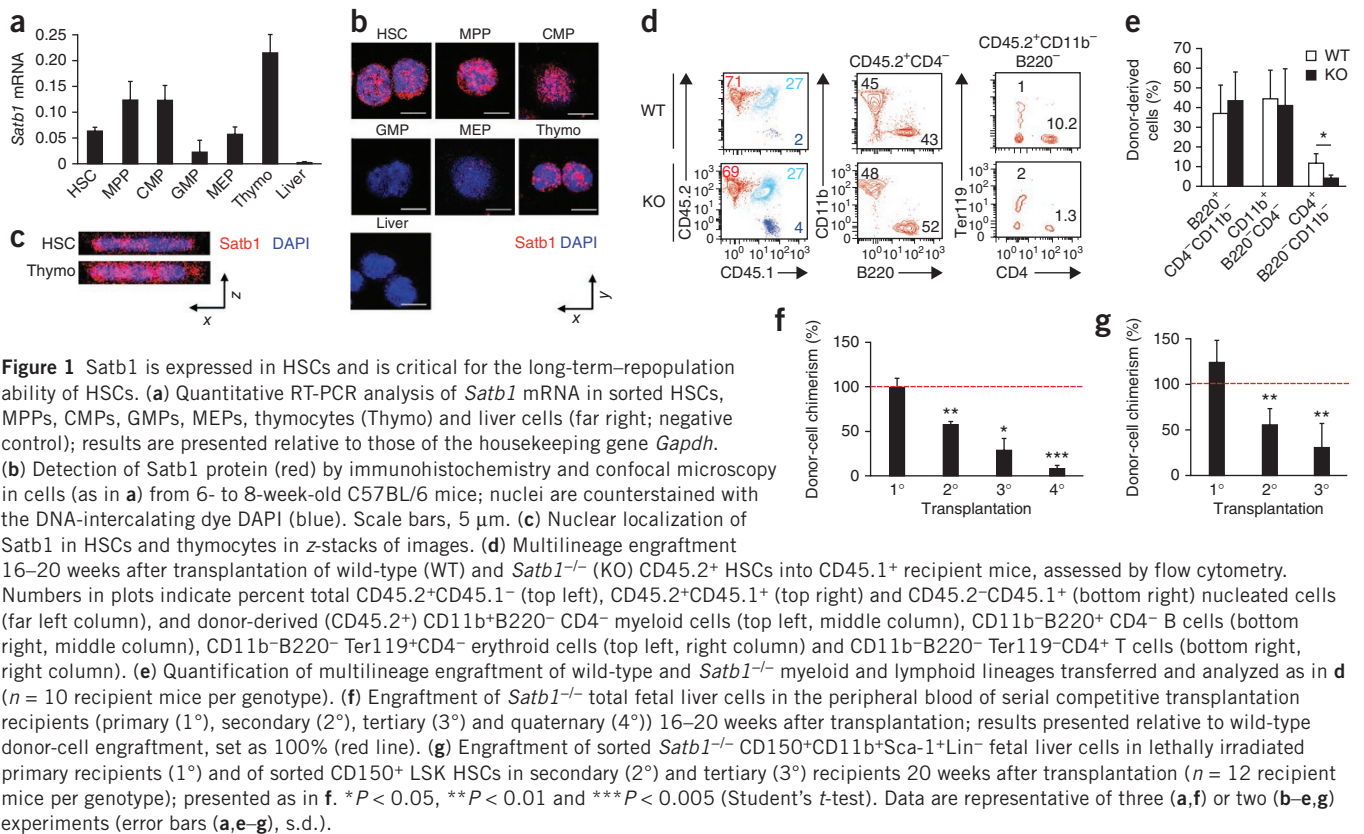
including HSCs[8,10,11]. However, it is still largely unknown how specific epigenetic factors affect and integrate the activation and repression of genes of various transcriptional programs in stem cells.

Satb1 ('special AT-rich sequence–binding protein 1') was identified as a chromatin organizer that forms cage-like chromatin networks in the nucleus of precursors of T cells, tethering together specific DNA sequences and regulating the expression of several genes that encode molecules relevant for T cell maturation[12–14]. Satb1 also functions in the differentiation of other hematopoietic lineages[15] and embryonic stem cells by controlling the expression of genes enoding transcriptional master regulators, such as *Sfpi1* (ref. 15) or *Nanog*[16]. Several studies have also linked Satb1 with cancer. Enhanced activity of this epigenetic factor is able to reprogram transcriptional networks and promote aberrant growth and metastasis in various types of epithelial tumors[17–19]. Additionally, impairment of Satb1 is associated with a subtype of acute myelogenous leukemia[15]. The role of Satb1 in tissue-specific stem cells, including HSCs, has not been examined thus far.

Here we investigated the role of Satb1 in HSCs and found that Satb1 critically mediated many functionally linked HSC properties. Satb1 was crucial for the maintenance of HSC self-renewal and exerted its function by simultaneously regulating transcriptional programs associated with the cell-polarity factor Numb, the stem-cell regulator c-Myc and several cell-cycle regulators, and thereby promoted the quiescence and repressed the lineage commitment of HSCs.

[1]Department of Cell Biology, Albert Einstein College of Medicine, Bronx, New York, USA. [2]Ruth L. and David S. Gottesman Institute for Stem Cell and Regenerative Medicine Research, Albert Einstein College of Medicine, Bronx, New York, USA. [3]Department of Medicine, Weill Cornell Medical College, New York, New York, USA. [4]Department of Developmental and Molecular Biology, Albert Einstein College of Medicine, Bronx, New York, USA. [5]Department of Medicine (Oncology), Albert Einstein College of Medicine, Bronx, New York, USA. [6]Albert Einstein Cancer Center, Albert Einstein College of Medicine, Bronx, New York, USA. [7]Department of Pathology, University of Michigan Medical School, Ann Arbor, Michigan, USA. Correspondence should be addressed to U.S. (ulrich.steidl@einstein.yu.edu).

Figure 1 Satb1 is expressed in HSCs and is critical for the long-term–repopulation ability of HSCs. (**a**) Quantitative RT-PCR analysis of *Satb1* mRNA in sorted HSCs, MPPs, CMPs, GMPs, MEPs, thymocytes (Thymo) and liver cells (far right; negative control); results are presented relative to those of the housekeeping gene *Gapdh*. (**b**) Detection of Satb1 protein (red) by immunohistochemistry and confocal microscopy in cells (as in **a**) from 6- to 8-week-old C57BL/6 mice; nuclei are counterstained with the DNA-intercalating dye DAPI (blue). Scale bars, 5 μm. (**c**) Nuclear localization of Satb1 in HSCs and thymocytes in *z*-stacks of images. (**d**) Multilineage engraftment 16–20 weeks after transplantation of wild-type (WT) and *Satb1*$^{-/-}$ (KO) CD45.2$^+$ HSCs into CD45.1$^+$ recipient mice, assessed by flow cytometry. Numbers in plots indicate percent total CD45.2$^+$CD45.1$^-$ (top left), CD45.2$^+$CD45.1$^+$ (top right) and CD45.2$^-$CD45.1$^+$ (bottom right) nucleated cells (far left column), and donor-derived (CD45.2$^+$) CD11b$^+$B220$^-$ CD4$^-$ myeloid cells (top left, middle column), CD11b$^-$B220$^+$CD4$^-$ B cells (bottom right, middle column), CD11b$^-$B220$^-$ Ter119$^+$CD4$^-$ erythroid cells (top left, right column) and CD11b$^-$B220$^-$Ter119$^-$CD4$^+$ T cells (bottom right, right column). (**e**) Quantification of multilineage engraftment of wild-type and *Satb1*$^{-/-}$ myeloid and lymphoid lineages transferred and analyzed as in **d** (*n* = 10 recipient mice per genotype). (**f**) Engraftment of *Satb1*$^{-/-}$ total fetal liver cells in the peripheral blood of serial competitive transplantation recipients (primary (1°), secondary (2°), tertiary (3°) and quaternary (4°)) 16–20 weeks after transplantation; results presented relative to wild-type donor-cell engraftment, set as 100% (red line). (**g**) Engraftment of sorted *Satb1*$^{-/-}$ CD150$^+$CD11b$^+$Sca-1$^+$Lin$^-$ fetal liver cells in lethally irradiated primary recipients (1°) and of sorted CD150$^+$ LSK HSCs in secondary (2°) and tertiary (3°) recipients 20 weeks after transplantation (*n* = 12 recipient mice per genotype); presented as in **f**. *P < 0.05, **P < 0.01 and ***P < 0.005 (Student's *t*-test). Data are representative of three (**a**,**f**) or two (**b**–**e**,**g**) experiments (error bars (**a**,**e**–**g**), s.d.).

RESULTS

Satb1 deficiency impairs the long-term repopulation ability of HSCs

To characterize the expression of *Satb1* mRNA and Satb1 protein in immature hematopoietic cells, we purified mouse HSCs (CD150$^+$ lineage-negative (Lin$^-$) c-Kit$^+$Sca-1$^+$ (LSK)), multipotent progenitor cells (MPPs; CD150$^-$ LSK), common myeloid progenitor cells (CMPs; CD34$^+$FcγRII/III$^-$c-Kit$^+$Sca-1$^-$Lin$^-$), granulocytic-monocytic progenitor cells (GMPs; CD34$^+$FcγRII/III$^+$c-Kit$^+$Sca-1$^-$Lin$^-$) and megakaryocytic-erythroid progenitor cells (MEPs; CD34$^-$FcγRII/III$^-$c-Kit$^+$Sca-1$^-$Lin$^-$) and analyzed them by quantitative RT-PCR and immunohistochemistry (sorting strategy, **Supplementary Fig. 1a**). We found high expression of *Satb1* mRNA and Satb1 protein in thymocytes and well-detectable expression of these in all bone marrow–derived stem cells and progenitor cells (**Fig. 1a**,**b**). Among the immature hematopoietic cell populations, Satb1 expression was highest in the HSC, MPP and CMP compartments and lower in lineage-restricted GMPs and MEPs. Satb1 was located in the nucleus in HSCs, as assessed by confocal microscopy (**Fig. 1c**). Satb1 has been reported to be present in the nucleus of thymocytes and has been shown to act as a transcriptional regulator[20,21].

To assess the role of Satb1 in HSC function, we examined the multilineage reconstitution and long-term self-maintenance ability of HSCs through the use of a *Satb1*$^{-/-}$ mouse model in which the first five of eleven exons (which encode 213 amino acids), including the translation start codon, are eliminated, which results in a complete lack of Satb1 protein[12]. We first characterized fetal hematopoiesis, as homozygous *Satb1*$^{-/-}$ mice die around the time of birth. Flow cytometry showed a normal frequency of HSCs, MPPs, CMPs, GMPs and MEPs in the fetal liver at embryonic days 17–18.5 (E17–18.5; **Supplementary Fig. 1b**). Colony assays showed that *Satb1*$^{-/-}$ fetal livers had significantly more functional colony-initiating progenitors

of the granulocytic-monocytic lineage (2.2-fold ± 0.6-fold;), erythroid lineage (4.3-fold ± 1.9-fold) and monocytic lineage (15.5-fold ± 7.1-fold) than did wild-type livers (*P* < 0.05; **Supplementary Fig. 1c**). Noncompetitive transplantation of *Satb1*$^{-/-}$ and wild-type fetal liver cells into wild-type congenic mice resulted in similar hematopoietic reconstitution 24 weeks after transplantation (**Supplementary Fig. 1d**) with no significant effect on the reconstitution of mature myeloid cells, erythroid cells or B cells (**Fig. 1d**,**e**); we found only slightly fewer CD4$^+$ T cells, consistent with published observations[12]. The frequency of functional HSCs in fetal livers at E17–18.5 was also not significantly altered by the absence of *Satb1*, as determined by competitive limiting-dilution transplantation assays (*P* > 0.05; **Supplementary Fig. 1e**). These findings showed that during embryogenesis, Satb1 was not essential for the generation of HSCs or for their short-term multilineage repopulation capacity.

To evaluate the long-term self-renewal ability of HSCs in the absence of Satb1, we did competitive serial transplantation experiments[22]. Unfractionated *Satb1*$^{-/-}$ cells from the fetal liver showed a progressive repopulation defect in serial competitive transplantations, with 42% ± 2.4% less repopulation than that of wild-type cells in the second reconstitution, 71.3% ± 12.9% less repopulation in the third transfer and 91.3% ± 2.7% less repopulation in the fourth serial transfer (**Fig. 1f** and **Supplementary Fig. 2a**). Serial transplantation of purified *Satb1*$^{-/-}$ HSCs also showed a progressive loss of repopulation ability relative to that of wild-type HSCs, with a 44% ± 15% less repopulation in the second serial transfer and 69% ± 25% less repopulation in the third serial transfer (**Fig. 1g** and **Supplementary Fig. 2b**). Characterization of the repopulation of various cell lineages showed a reconstitution impairment in all compartments (**Supplementary Fig. 2c**), indicative of a defect at the stem-cell level. Together these data showed that Satb1 was indispensable for the long-term self-renewal of HSCs

Figure 2 *Satb1* deficiency leads to less HSC quiescence. (**a**) Cell-cycle distribution of wild-type and *Satb1$^{-/-}$* LSK HSCs 20–24 weeks after their transplantation into BL6/SJL mice, assessed by flow cytometry analysis of the intercalation of Pyronin Y and Hoechst 33342. Numbers in outlined areas indicate percent cells in each phase of the cell cycle. (**b**) Quantification of LSK cells in phases G0, G1 and S-G2-M of the cell cycle ($n = 2$ samples per genotype). (**c**) Quantification of CD150$^+$ LSK HSCs in phases G0, G1 and S-G2-M of the cell cycle ($n = 2$ per genotype). (**d**) Division assay of CD150$^+$CD48$^-$ LSK HSCs sorted and individually deposited into Terasaki plates, presented as percent wells containing 1, 2 or >2 cells after culture of a single HSC in each ($n = 120$ cells per genotype). Red asterisk, *$P < 0.05$ for G0, blue asterisk, *$P < 0.05$ for G1. *$P < 0.05$ and **$P < 0.01$ (Student's *t*-test). Data are representative of two experiments (average and s.d. in **b**–**d**).
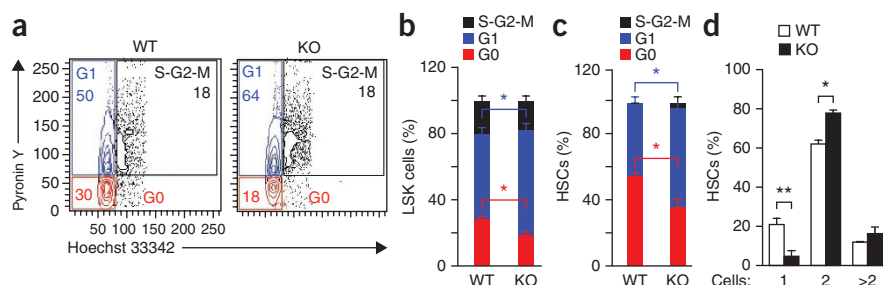
and that the absence of Satb1 led to a progressive decrease in the abundance of functional HSCs.

Satb1-deficient HSCs are less quiescent

Maintenance of a quiescent state is an important feature of HSCs, and loss of quiescence has been shown to lead to the loss of functional HSCs[23]. To determine whether Satb1 regulates HSC quiescence, we quantified quiescent and actively cycling wild-type and *Satb1$^{-/-}$* cells by analyzing the intercalation of Hoechst 33342 and Pyronin Y[24] in the immature LSK (Lin$^-$Sca-1$^+$c-Kit$^+$) compartment (**Fig. 2a,b**) as well as the HSC compartment (**Fig. 2c**). In both stem cell–containing populations, there were significantly fewer quiescent cells in the G0 phase of the cell cycle in the absence of *Satb1* (**Fig. 2b,c**). However, most apparent differences in cell-cycle distribution were in the purified HSC population; 36% ± 4.5% of *Satb1$^{-/-}$* HSCs were in G0, compared with 53.5% ± 2.1% wild-type HSCs, whereas significantly more *Satb1$^{-/-}$* HSCs (63% ± 5.7%) than wild-type HSCs (42.5% ± 3.5%) were in G1 **Fig. 2c**). Consistent with that, the alteration in cell-cycle activity was accompanied by a change in cell-division kinetics. In experiments with individually sorted, highly enriched HSCs (CD150$^+$CD48$^-$ LSK HSCs), significantly fewer *Satb1$^{-/-}$* HSCs (5% ± 2.4%) than wild-type HSCs (20.7% ± 3.4%) remained in an

undivided state, whereas significantly more *Satb1$^{-/-}$* HSCs (77.5% ± 1.2%) than wild-type HSCs (61.5% ± 1.2%) divided once after 48 h in an *ex vivo* culture assay (**Fig. 2d**). Consistent with that, we found that *Satb1* expression in wild-type HSCs was dependent on the cell-cycle phase, with highest *Satb1* expression in cells in G0 (**Supplementary Fig. 2d**). *Satb1* expression in HSCs was much lower after HSC activation *in vivo* after treatment with 5-fluorouracil than in nonactivated HSCs at steady state (**Supplementary Fig. 2e**). Together these results indicated that Satb1 promoted the quiescence of HSCs under steady-state as well as stress conditions.
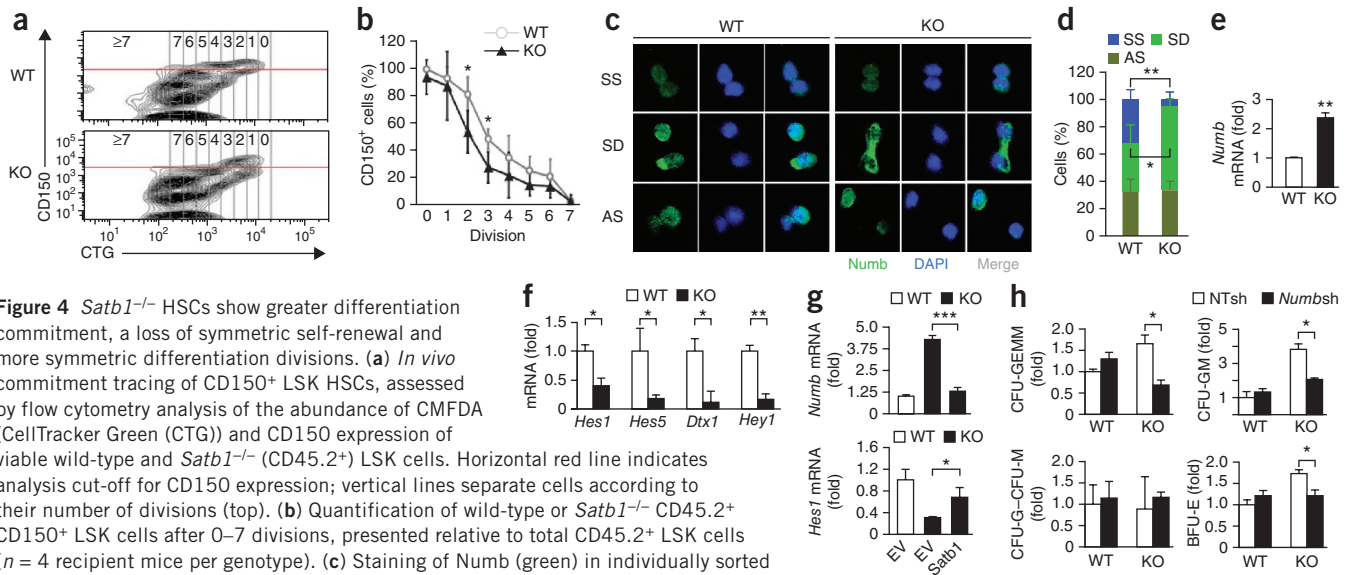
Greater differentiation commitment of Satb1-deficient HSCs

To further elucidate the functional alterations of adult *Satb1$^{-/-}$* HSCs, we characterized the composition of the HSC (CD150$^+$CD48$^-$ LSK) and MPP (CD150$^-$CD48$^+$ LSK) compartments of wild-type and *Satb1$^{-/-}$* cells after competitive congenic transplantation into BL6/SJL mice. Recipients of unfractionated *Satb1$^{-/-}$* fetal liver cells had a significantly lower frequency of HSCs (4.2% ± 3.6%) than did recipients of wild-type cells (13.9% ± 11.6%) and had a significantly higher frequency of MPPs (77.5% ± 12.9%) than did recipients of wild-type cells (61.4% ± 16.9%; **Fig. 3a,b**). Quantification of HSCs and MPPs also showed that recipients of *Satb1$^{-/-}$* cells had significantly fewer
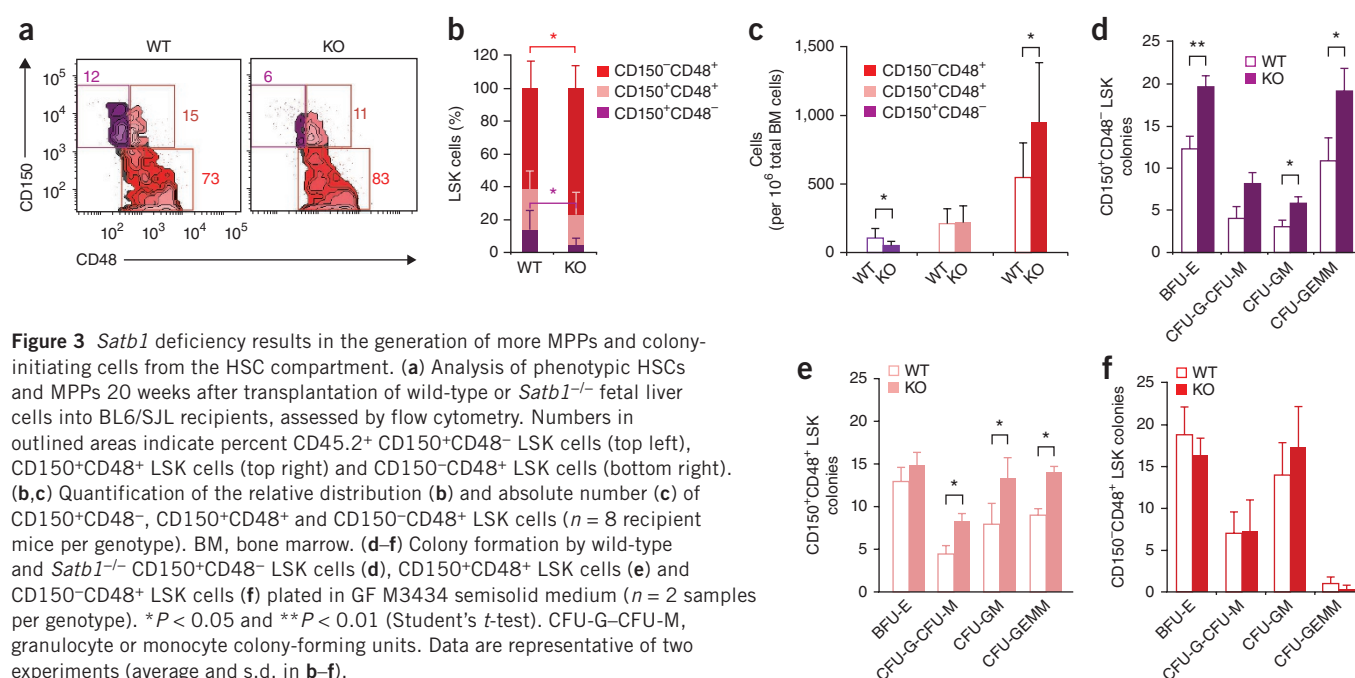
Figure 3 *Satb1* deficiency results in the generation of more MPPs and colony-initiating cells from the HSC compartment. (**a**) Analysis of phenotypic HSCs and MPPs 20 weeks after transplantation of wild-type or *Satb1$^{-/-}$* fetal liver cells into BL6/SJL recipients, assessed by flow cytometry. Numbers in outlined areas indicate percent CD45.2$^+$ CD150$^+$CD48$^-$ LSK cells (top left), CD150$^+$CD48$^+$ LSK cells (top right) and CD150$^-$CD48$^+$ LSK cells (bottom right). (**b,c**) Quantification of the relative distribution (**b**) and absolute number (**c**) of CD150$^+$CD48$^-$, CD150$^+$CD48$^+$ and CD150$^-$CD48$^+$ LSK cells ($n = 8$ recipient mice per genotype). BM, bone marrow. (**d**–**f**) Colony formation by wild-type and *Satb1$^{-/-}$* CD150$^+$CD48$^-$ LSK cells (**d**), CD150$^+$CD48$^+$ LSK cells (**e**) and CD150$^-$CD48$^+$ LSK cells (**f**) plated in GF M3434 semisolid medium ($n = 2$ samples per genotype). *$P < 0.05$ and **$P < 0.01$ (Student's *t*-test). CFU-G–CFU-M, granulocyte or monocyte colony-forming units. Data are representative of two experiments (average and s.d. in **b**–**f**).

Figure 4 $Satb1^{-/-}$ HSCs show greater differentiation commitment, a loss of symmetric self-renewal and more symmetric differentiation divisions. (**a**) *In vivo* commitment tracing of CD150+ LSK HSCs, assessed by flow cytometry analysis of the abundance of CMFDA (CellTracker Green (CTG)) and CD150 expression of viable wild-type and $Satb1^{-/-}$ (CD45.2+) LSK cells. Horizontal red line indicates analysis cut-off for CD150 expression; vertical lines separate cells according to their number of divisions (top). (**b**) Quantification of wild-type or $Satb1^{-/-}$ CD45.2+ CD150+ LSK cells after 0–7 divisions, presented relative to total CD45.2+ LSK cells ($n = 4$ recipient mice per genotype). (**c**) Staining of Numb (green) in individually sorted wild-type and $Satb1^{-/-}$ CD150+ LSK cells after one division, to identify symmetric self-renewal (SS), symmetric differentiation (SD) and asymmetric (AS) division. DNA was counterstained with DAPI (blue). (**d**) Symmetric and asymmetric divisions of wild-type and $Satb1^{-/-}$ CD45.2+CD150+ LSK cells 24 weeks after transplantation into BL6/SJL recipient mice ($n = 75$ (wild-type) or 85 ($Satb1^{-/-}$) cell doublets). (**e**) Quantitative RT-PCR analysis of *Numb* mRNA in wild-type and $Satb1^{-/-}$ CD150+CD48− LSK cells ($n = 2$ recipient mice per genotype); results are normalized to *Gapdh* and are presented relative to those of wild-type HSCs. (**f**) Quantitative RT-PCR analysis of mRNA of the Notch target genes *Hes1*, *Hes5*, *Dtx1* and *Hey1* in wild-type and $Satb1^{-/-}$ CD150+ LSK cells ($n = 3$ recipients per genotype); results are normalized to *Gapdh* and are presented relative to those of wild-type cells. (**g**) Quantitative RT-PCR analysis of *Numb* and *Hes1* mRNA after lentiviral transduction of wild-type and $Satb1^{-/-}$ CD150+CD48− LSK cells with empty vector (EV) or a Satb1-expressing vector (Satb1); results are normalized to *Gapdh* and are presented relative to those of wild-type cells transduced with empty vector. (**h**) Colony assay of wild-type and $Satb1^{-/-}$ CD150+CD48− LSK cells ($n = 2$ recipients per genotype) transduced with lentiviral constructs expressing *Numb*-specific shRNA (*Numb*sh) or nontargeting shRNA (NTsh); results are relative to those of wild-type HSCs transduced with nontargeting shRNA. *$P < 0.05$, **$P < 0.01$ and ***$P < 0.005$ (Student's *t*-test). Data are representative of two (**a**,**e**–**h**) or three (**c**,**d**) experiments (average and s.d. in **b**,**d**–**g**).

HSCs (46 ± 40 cells ($Satb1^{-/-}$) versus 107 ± 71 cells (wild-type) per 10^6 total nucleated bone marrow cells) and significantly more MPPs (944 ± 446 cells ($Satb1^{-/-}$) versus 549 ± 254 cells (wild-type) per 10^6 total nucleated bone marrow cells) than did recipients of wild-type cells (**Fig. 3c**).

To determine if $Satb1^{-/-}$ HSCs were more prone to commit to differentiation, we evaluated the colony-formation capacity of fractionated CD150+CD48− LSK cells, CD150+CD48+ LSK cells and CD150−CD48+ LSK MPPs. $Satb1^{-/-}$ CD150+CD48− LSK cells formed 1.6-fold more erythroid burst colony-forming units (BFU-E), 1.9-fold more granulocyte-monocyte colony-forming units (CFU-GM) and 1.8-fold more granulocyte-erythrocyte-monocyte-megakaryocyte colony-forming units (CFU-GEMM) than did their wild-type counterparts (**Fig. 3d**). Similarly, $Satb1^{-/-}$ CD150+CD48+ LSK cells also showed 1.7-fold more generation of CFU-GM, 1.8-fold more generation of CFU-G or M and 1.6-fold more generation of CFU-GEMM than did their wild-type counterparts (**Fig. 3e**). That enhanced formation of myeloid colonies by $Satb1^{-/-}$ cells was restricted to the HSC compartments, as we did not observe a substantial difference in the colony formation of $Satb1^{-/-}$ MPPs versus wild-type MPPs (**Fig. 3f**). These findings suggested that Satb1 suppressed differentiation commitment specifically in HSCs.

To further assess the role of Satb1 in HSC commitment, we modified a published method for tracing cell divisions in stem cells and progenitor cells *in vivo*[25]. Here, we purified donor-derived $Satb1^{-/-}$ and wild-type CD150+ LSK cells from long-term–reconstituted recipient mice and labeled them with the cell-division tracer CMFDA. We then transplanted those cells into a second cohort of sublethally irradiated recipients and assessed them by monitoring the division and expression of the signaling-lymphocytic-activation-molecule

family member CD150 of individual donor-derived HSCs (**Fig. 4a**). We used CD150 as a marker because it has been shown that HSCs downregulate CD150 expression after commitment to differentiation[26,27]. Applying this strategy, we found that $Satb1^{-/-}$ CD150+ LSK HSCs downregulated CD150 expression after fewer cell divisions after transplantation relative to the downregulation of its expression by wild-type HSCs (**Fig. 4a,b**). After two divisions, $54.3\% \pm 15.5\%$ of $Satb1^{-/-}$ HSCs versus $81.2\% \pm 12.5\%$ of wild-type HSCs still expressed CD150. After three divisions, $28.6\% \pm 11.4\%$ of the $Satb1^{-/-}$ HSCs versus $48.8\% \pm 7.4\%$ of the wild-type HSCs expressed CD150 (**Fig. 4b**). These observations indicated that HSC commitment was quantitatively greater in the absence of Satb1.

Satb1 regulates the fate of HSCs by modulating the division mode
The impairment of long-term–repopulation capacity and the greater commitment of $Satb1^{-/-}$ HSCs led us to hypothesize that Satb1 regulates the division mode of HSCs by promoting symmetric self-renewal divisions and repressing differentiation divisions. To assess this, we quantified symmetric and asymmetric divisions in individual $Satb1^{-/-}$ and wild-type HSCs by staining the cell-fate determinant and polarity factor Numb as described before[28,29]. Higher expression of Numb protein in one of two daughter cells indicated asymmetric division and high Numb expression in both daughter cells showed symmetric differentiation division, whereas sustained low expression of Numb in both daughter cells marked symmetric self-renewal divisions (**Fig. 4c**). We quantified the division types of individual HSCs and found that $Satb1^{-/-}$ HSCs underwent significantly fewer symmetric self-renewal divisions ($5.2\% \pm 5.4\%$) than did wild-type HSCs ($32.4\% \pm 7.2\%$; a difference of 6.2-fold), whereas $Satb1^{-/-}$ HSCs underwent significantly more symmetric differentiation divisions ($61.4\% \pm 5.5\%$)

than did wild-type HSCs (35.2% ± 13.5%; **Fig. 4d**). These observations showed that *Satb1* promoted the self-renewal and suppressed the differentiation commitment of HSCs by regulating the type of stem-cell division.

Satb1 regulates Notch targets through repression of *Numb* in HSCs

Regulation of Numb has been reported mainly at the protein level[30,31]; *Numb* has also been found to be transcriptionally regulated in *Drosophila* sensory bristle cells[32]. Transcriptional or epigenetic regulation of *Numb* in mammalian stem cells is unknown. We found twofold higher *Numb* mRNA expression in *Satb1*^{−/−} CD150^{+}CD48^{−} LSK HSCs than in their wild-type counterparts (**Fig. 4e**). Numb is a negative regulator of Notch signaling that has been reported to modulate cell-fate 'decisions' of HSCs[30,31]. We therefore assessed whether the higher *Numb* expression in the absence of *Satb1* had an effect on the transcription of genes targeted by Notch. We found that *Satb1*^{−/−} CD150^{+} LSK HSCs, as well as highly purified *Satb1*^{−/−} CD150^{+}CD48^{−} LSK HSCs, had significantly lower expression of Notch targets, including *Hes1* (60% ± 13%), *Hes5* (82.5% ± 6.6%), *Dtx1* (88.5% ± 19.4%) and *Hey1* (83.4% ± 9.2%), than did their wild-type counterparts (**Fig. 4f** and **Supplementary Fig. 3a,b**). To further assess whether Numb was downstream of Satb1 and whether higher *Numb* expression was functionally critical for the altered fate of *Satb1*^{−/−} HSCs, we did 'rescue' experiments (**Fig. 4g,h**). Ectopic re-expression of Satb1 in Satb1-deficient HSCs to expression similar to that in wild-type HSCs led to restoration of *Numb* expression as well as of *Hes1* expression (**Fig. 4g** and **Supplementary Fig. 3c**). Moreover, short hairpin RNA (shRNA)-mediated knockdown of the higher expression of *Numb* in *Satb1*^{−/−} CD150^{+}CD48^{−} LSK HSCs by 60% ± 3.1% led to a significant decrease in the greater abundance of colony-initiating cells by diminishing the CFU-GEMM (58.2% ± 6.7%), CFU-GM (45.8% ± 2%) and BFU-E (30% ± 8%) compared with that of cells transduced with nontargeting control shRNA (**Fig. 4h** and **Supplementary Fig. 3d**). Consistent with that observation, the expression of *Hes1*, *Hes5* and *Dtx1* was de-repressed in *Satb1*^{−/−} CD150^{+}CD48^{−} LSK cells expressing Numb-specific shRNA relative to the expression of those genes in their counterparts transduced with nontargeting control shRNA (2.9-fold ± 0.2-fold, 2.8-fold ± 0.4-fold and 4.3-fold ± 0.8-fold, respectively; **Supplementary Fig. 3e**). Notably, shRNA-mediated knockdown of *Numb* in wild-type HSCs did not cause a significant change in the number of colony-initiating cells (**Fig. 4h**). These results demonstrated that Satb1 modulated the fate determination of HSCs at least in part by regulating *Numb* expression and Notch signaling. The finding that downregulation of *Numb* was sufficient to 'rescue' the enhanced differentiation commitment of *Satb1*^{−/−} HSCs but did not have an effect on wild-type HSCs suggested that additional mechanisms contributed to the changes in the fate of Satb1-deficient HSCs.

Satb1 deficiency alters transcriptional networks in HSCs

To obtain insight into potential cooperating factors that contributed to the enhanced differentiation commitment of Satb1-deficient HSCs, we measured gene-expression changes in *Satb1*^{−/−} HSCs. Microarray analysis identified 631 genes with different expression by comparison of adult *Satb1*^{−/−} HSCs and adult wild-type HSCs (**Supplementary Table 1**); of those, 73.3% had higher expression and 26.3% had lower expression in *Satb1*^{−/−} HSCs than in wild-type HSCs, which supported the proposal of a role for Satb1 as an overall transcriptional repressor in HSCs. Ingenuity pathway analysis showed considerable enrichment for Satb1-dependent genes in networks that regulate cellular assembly and organization and the cell cycle (**Supplementary Fig. 4a**). We confirmed the altered expression of a subset of genes

from both categories by real-time PCR analysis of an independent set of samples. We confirmed significant overexpression in *Satb1*^{−/−} HSCs (relative to expression in wild-type HSCs) of genes encoding molecules involved in cell-cycle activation (*Rbbp9*, 3.5-fold ± 1-fold; *Kdm3a*, 2.2-fold ± 0.3-fold; *Chaf1a*, 3.9-fold ± 1.4-fold; and *Bgn*, 31.1-fold ± 5-fold) and genes encoding molecules that regulate cellular organization and contribute to cellular polarity (*Iptr1*, 2.1-fold ± 0.46-fold; and *Tnik*, 1.8-fold ± 0.2-fold; *P* <0.05; **Supplementary Fig. 4b**). These data showed that Satb1 regulated various functional gene networks in HSCs that were supportive of the observed phenotype of enhanced cell-cycle activity and differentiation commitment of *Satb1*^{−/−} HSCs.
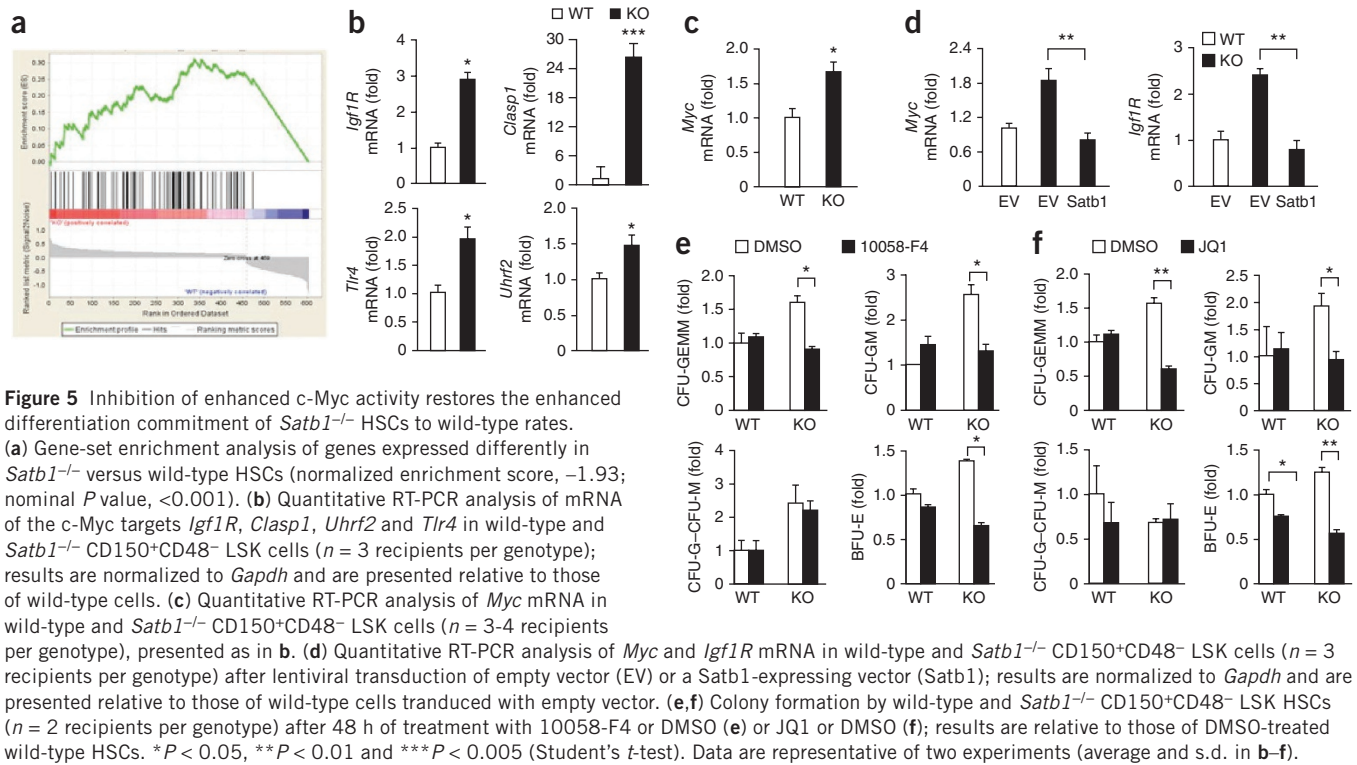
Gene-set enrichment analysis[33] of genes expressed differently in *Satb1*^{−/−} HSCs relative to their expression in wild-type HSCs identified a core set of genes directly targeted by c-Myc[34] with greater abundance in *Satb1*^{−/−} HSCs (normalized enrichment score, 1.90; nominal *P* value, <0.001; **Fig. 5a** and **Supplementary Fig. 4c**). Quantitative real-time PCR showed overexpression in *Satb1*^{−/−} CD150^{+}CD48^{−} LSK HSCs (relative to expression in wild-type HSCs) of several targets of c-Myc, including *Igf1R* (2.9-fold ± 0.2-fold), *Clasp1* (26.1-fold ± 3.0-fold), *Tlr4* (1.9-fold ± 0.2-fold) and *Uhrf2* (1.47-fold ± 0.2-fold; **Fig. 5b**), as well as *Myc* itself (1.66-fold ± 0.2-fold; **Fig. 5c**). To assess whether c-Myc was downstream of Satb1, as has been shown in T cells[21], we measured *Myc* expression in *Satb1*^{−/−} HSCs after lentiviral re-expression of Satb1. Restoration of Satb1 expression in Satb1-deficient CD150^{+}CD48^{−} LSK HSCs led to normalization of the expression of *Myc* and of the c-Myc target *Igfr1* (**Fig. 5d**). These data showed that Satb1 regulated transcriptional networks involved in cell-cycle regulation and cellular organization in HSCs.

Greater *Myc* activity in *Satb1*^{−/−} HSCs

To determine whether the Satb1-dependent increase in c-Myc activity was functionally relevant in *Satb1*^{−/−} HSCs, we treated Satb1-deficient CD150^{+}CD48^{−} LSK HSCs with two different small-molecule inhibitors of c-Myc (10058-F4, shown to specifically interfere with c-Myc transactivation[35], and JQ1, a bromodomain-BRD4 inhibitor that causes direct repression of *Myc* transcription[36]) and assessed colony-initiating capacity. Both 10058-F4 and JQ1 impaired the expression of genes targeted by c-Myc (**Supplementary Fig. 5a,b**) and the colony formation of Satb1-deficient HSCs (**Supplementary Fig. 5c,d**) in a dose-dependent manner. We then assessed the effect of a low effective inhibitor concentration (15 μM 10058-F4 and 250 nM JQ1) on *Satb1*^{−/−} and wild-type HSCs. We found less generation of CFU-GEMM (39% ± 1.9%) CFU-GM (48.9% ± 8%) and BFU-E (45% ± 2.8%) by Satb1-deficient HSCs treated with 10058-F4 than by their counterparts treated with DMSO (dimethyl sulfoxide) and less generation of CFU-GEMM (56.8% ± 1.9%), CFU-GM (51% ± 5.6%) and BFU-E (47.2% ± 2.7%) by Satb1-deficient HSCs treated with JQ1 than by their DMSO-treated counterparts (**Fig. 5e,f**), which demonstrated 'rescue' of the greater abundance of colony-forming units. We did not observe an effect of these inhibitors on wild-type CD150^{+}CD48^{−} LSK HSCs (**Fig. 5e,f**). These results showed that greater c-Myc activity was functionally important in *Satb1*^{−/−} HSCs. Of note, *Numb* expression was not significantly altered after treatment of *Satb1*^{−/−} HSCs with inhibitors of c-Myc (*P* >0.05; **Supplementary Fig. 5e**).

Widespread epigenetic changes in Satb1-deficient HSCs

We assessed whether Satb1 binds to the promoter regions of *Numb* and *Myc* in HSCs by chromatin immunoprecipitation (ChIP) with a hematopoietic stem cell line (HPC7)[37]. We found that Satb1 bound

Figure 5 Inhibition of enhanced c-Myc activity restores the enhanced differentiation commitment of $Satb1^{-/-}$ HSCs to wild-type rates. (**a**) Gene-set enrichment analysis of genes expressed differently in $Satb1^{-/-}$ versus wild-type HSCs (normalized enrichment score, −1.93; nominal P value, <0.001). (**b**) Quantitative RT-PCR analysis of mRNA of the c-Myc targets $Igf1R$, $Clasp1$, $Uhrf2$ and $Tlr4$ in wild-type and $Satb1^{-/-}$ CD150+CD48− LSK cells (n = 3 recipients per genotype); results are normalized to $Gapdh$ and are presented relative to those of wild-type cells. (**c**) Quantitative RT-PCR analysis of Myc mRNA in wild-type and $Satb1^{-/-}$ CD150+CD48− LSK cells (n = 3-4 recipients per genotype), presented as in **b**. (**d**) Quantitative RT-PCR analysis of Myc and $Igf1R$ mRNA in wild-type and $Satb1^{-/-}$ CD150+CD48− LSK cells (n = 3 recipients per genotype) after lentiviral transduction of empty vector (EV) or a Satb1-expressing vector (Satb1); results are normalized to $Gapdh$ and are presented relative to those of wild-type cells tranduced with empty vector. (**e**,**f**) Colony formation by wild-type and $Satb1^{-/-}$ CD150+CD48− LSK HSCs (n = 2 recipients per genotype) after 48 h of treatment with 10058-F4 or DMSO (**e**) or JQ1 or DMSO (**f**); results are relative to those of DMSO-treated wild-type HSCs. *P < 0.05, **P < 0.01 and ***P < 0.005 (Student's t-test). Data are representative of two experiments (average and s.d. in **b**–**f**).

to chromatin upstream of the transcriptional start sites of $Numb$ and Myc (**Fig. 6a,b** and **Supplementary Fig. 6a,b**). As Satb1-dependent gene regulation has been linked to epigenetic modifications, such as histone modifications and DNA cytosine methylation[16,21], we analyzed permissive (H3K4me3) and repressive (H3K27me3) histone marks at the $Numb$ and Myc promoters. ChIP of primary $Satb1^{-/-}$ and wild-type HSCs showed that in the absence of Satb1, there were significantly more H3K4me3 marks at the promoter regions of both $Numb$ and Myc (**Fig. 6c,d**), in line with the higher expression of $Numb$ and Myc in $Satb1^{-/-}$ HSCs.

We further evaluated genome-wide DNA cytosine methylation by enhanced reduced representation bisulfite sequencing (ERRBS) of DNA extracted from sorted HSCs and MPPs. We found significant differences between $Satb1^{-/-}$ HSCs and wild-type HSCs in DNA cytosine methylation, with a total of 11,924 differently methylated regions (DMRs; 1-kilobase genomic tiles with no overlap) composed of 5,089 hypomethylated DMRs and 6,835 hypermethylated DMRs in $Satb1^{-/-}$ HSCs relative to their methylation in wild-type HSCs (**Fig. 6e** and **Supplementary Table 2**). DMRs associated with $Satb1^{-/-}$ HSCs were located mainly in CpG islands and isolated CpGs, without a strong
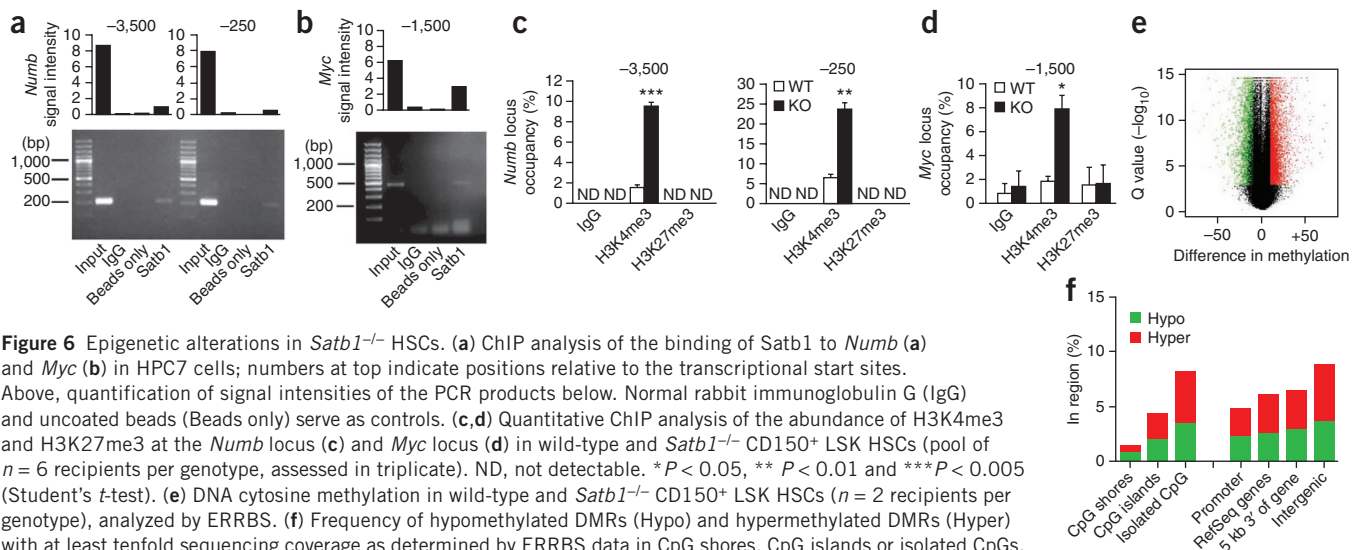
Figure 6 Epigenetic alterations in $Satb1^{-/-}$ HSCs. (**a**) ChIP analysis of the binding of Satb1 to $Numb$ (**a**) and Myc (**b**) in HPC7 cells; numbers at top indicate positions relative to the transcriptional start sites. Above, quantification of signal intensities of the PCR products below. Normal rabbit immunoglobulin G (IgG) and uncoated beads (Beads only) serve as controls. (**c**,**d**) Quantitative ChIP analysis of the abundance of H3K4me3 and H3K27me3 at the $Numb$ locus (**c**) and Myc locus (**d**) in wild-type and $Satb1^{-/-}$ CD150+ LSK HSCs (pool of n = 6 recipients per genotype, assessed in triplicate). ND, not detectable. *P < 0.05, ** P < 0.01 and ***P < 0.005 (Student's t-test). (**e**) DNA cytosine methylation in wild-type and $Satb1^{-/-}$ CD150+ LSK HSCs (n = 2 recipients per genotype), analyzed by ERRBS. (**f**) Frequency of hypomethylated DMRs (Hypo) and hypermethylated DMRs (Hyper) with at least tenfold sequencing coverage as determined by ERRBS data in CpG shores, CpG islands or isolated CpGs, as well as in various genomic features (promoter, gene regions from the reference sequence database of the National Center for Biotechnology Information (RefSeq genes) and 5 kb downstream (3′) of those (5 kb 3′ of gene), and intergenic regions), in $Satb1^{-/-}$ HSCs versus wild-type HSCs. Data are representative of one experiment (**a**,**b**) or two experiments (**c**–**f**; error bars (**c**,**d**), s.d.).

'preference' for a presence in specific genomic regions, but with a slightly greater abundance of DMRs in intergenic regions (**Fig. 6f**). Next we compared wild-type HSCs and wild-type MPPs to define methylation changes associated with normal HSC commitment. We identified a total of 14,778 HSC commitment–associated DMRs (**Supplementary Fig. 6c**), located mainly in CpG islands and isolated CpGs, and without a strong 'preference' for intergenic or intragenic regions (**Supplementary Fig. 6d**). When we compared those normal HSC commitment–associated DMRs with the DMRs identified in $Satb1^{-/-}$ HSCs, we found a significant overlap ($P = 1.2 \times 10^{-37}$ by hypergeometrical testing), with 37% shared hypermethylated DMRs and 15% shared hypomethylated DMRs (overall, 22% shared DMRs; **Supplementary Fig. 6e**).

We further evaluated whether methylation changes were accompanied by gene-expression changes in $Satb1^{-/-}$ HSCs and found a set of 67 genes with substantial alterations in both expression and methylation in the vicinity of the gene (**Supplementary Table 3**). Ingenuity pathway analysis showed enrichment in several functionally relevant networks (**Supplementary Fig. 6f** and **Supplementary Table 4**). Notably, among those was a subset of genes (*Itpr1* and *Tnik*) that encode molecules with known roles in cell cycle and cellular assembly[38,39], whose difference in expression in $Satb1^{-/-}$ HSCs we had confirmed (**Supplementary Fig. 4b**). Together these data showed that Satb1 acted as an epigenetic regulator in HSCs by modulating histone marks and DNA cytosine methylation, and indicated that $Satb1$ deficiency led to a commitment-primed epigenetic state in HSCs.

DISCUSSION

The interaction between transcription-factor networks is a key mechanism of cell-fate determination in pluripotent hematopoietic cells, including HSCs[40–42]. The biological outcome of the simultaneous activity of multiple transcriptional networks depends on the exact cellular and temporal context as HSCs commit and differentiate[40–42]. However, how transcriptional networks themselves are established and coordinately regulated in stem cells is still largely unknown. Our study has identified the chromatin-remodeling factor Satb1 as a regulator of transcriptional programs that 'instruct' quiescence, self-renewal and commitment in HSCs.

Quiescent HSCs have superior long-term engraftment potential relative to that of actively cycling HSCs[24,43]. Restriction of the cell cycling of HSCs prevents their premature depletion and hematopoietic failure under stress conditions[44]. Our study has shown that genes encoding molecules important for cell-cycle activation, including factors important in the transition from a quiescent stage (G0) to an active stage (G1), were derepressed in $Satb1^{-/-}$ HSCs. Consistent with those findings, $Satb1^{-/-}$ HSC populations were in a more activated state with significantly fewer cells in the G0 phase and more in the G1 phase of the cell cycle than were Satb1-expressing HSC populations. In contrast to G0, G1 is the cell-cycle phase in which intrinsic signals can influence cell fate. The integration and interpretation of transcriptional programs determine whether a cell enters S phase or pauses during G1 until the cell makes the 'decision' to self-renew, differentiate or undergo apoptosis[45]. The enhanced progression of $Satb1^{-/-}$ HSCs into G1 may alter their likelihood to undergo cell-fate specification by making them more susceptible to differentiation commitment–inducing factors. Notably, $Satb1^{-/-}$ HSCs had quantitatively greater generation of committed progenitor cells, which indicated that Satb1 was critical for suppressing HSC commitment and linked HSC quiescence with differentiation.

Chromatin-remodeling factors have been found to regulate cell fate in embryonic stem cells[39] and invertebrate stem cells[46]. We found that $Satb1^{-/-}$ HSCs underwent significantly more symmetric commitment divisions at the expense of symmetric self-renewal divisions, whereas the rate of asymmetric divisions remained unchanged. Two Satb1-dependent gene networks were directly involved in the regulation of cellular polarity, differentiation and proliferation. In $Satb1^{-/-}$ HSCs, expression of the genes encoding c-Myc and several of its transcriptional targets and the negative Notch regulator Numb was higher. Enforced expression or activation of c-Myc can lead to greater differentiation at the expense of self-renewal in HSCs[47]. Similarly, slightly higher Numb expression can also induce the differentiation of HSCs[29], which suggests that Satb1 inhibits differentiation commitment at least in part through repression of *Myc* and *Numb*. Indeed, independent Numb and Myc 'rescue' experiments showed that the combination of a greater abundance of both c-Myc and Numb was critical for the enhanced commitment of $Satb1^{-/-}$ HSC.

Numb is a segregating cell-fate determinant and tissue-specific repressor of the Notch pathway[30,31]. Numb-mediated suppression of Notch in HSCs can induce differentiation[29]. We found that Satb1 negatively regulated *Numb* expression in HSCs and that $Satb1$ deficiency led to Numb-mediated inhibition of the expression of genes targeted by Notch. Impairment of the Notch target genes *Hes1* and *Hes5* in HSCs results in loss of HSCs and overproduction of myeloid progenitor cells[48], consistent with the observed phenotype and results of functional 'rescue' experiments with $Satb1^{-/-}$ HSCs. Restoration of Satb1 expression in $Satb1^{-/-}$ HSCs led to normalization of the higher expression of *Numb* and significantly higher expression of *Hes1*. Furthermore, restoration of *Numb* expression normalized the expression of *Hes1*, *Hes5* and *Dtx1* and 'rescued' the greater colony-initiating capacity of $Satb1^{-/-}$ HSCs. These data showed that in the absence of $Satb1$, higher expression of *Numb* mediated the decrease in symmetrical self-renewal divisions and the concomitant greater production of MPPs, which ultimately depleted the pool of $Satb1^{-/-}$ HSCs.

In T cells, Satb1 binds to the *Myc* promoter and 'instructs' histone modifications[21]. We found that Satb1 bound to the promoters of both *Numb* and *Myc* in HPC7 cells, and restoration of Satb1 expression in $Satb1^{-/-}$ HSCs 'rescued' the higher expression of *Numb* and *Myc*. Those observations, together with the finding of higher expression of *Numb* and *Myc* in $Satb1^{-/-}$ HSCs, indicated that both Numb and c-Myc were downstream of Satb1. It is possible that this regulatory function of Satb1 is indirect and that cofactors are required.

Satb1 acts as an epigenetic regulator and chromatin organizer in T cells and erythroid cells[20] and is accompanied by alterations in histone modifications[16]. Our data showed that in $Satb1^{-/-}$ HSCs, the absence of Satb1 resulted in a greater abundance of permissive H3K4me3 mark at the promoters both *Numb* and *Myc*. In addition, the DNA cytosine methylation patterns in $Satb1^{-/-}$ HSCs were significantly different from those of wild-type HSCs; the patterns in $Satb1^{-/-}$ HSCs resembled those of wild-type MPPs and indicated a 'commitment-primed' epigenetic state of $Satb1^{-/-}$ HSCs. Those findings further supported our observation of greater differentiation commitment and less self-renewal of $Satb1^{-/-}$ HSCs and showed that Satb1 acted as an epigenetic regulator in HSCs by modulating histone marks and DNA cytosine methylation.

Impairment of Satb1 activity is associated with a subset of patients with acute myeloid leukemia[15]. Moreover, myeloid-biased hematopoiesis has been noted in mouse loss-of-function models of positive Notch regulators, and loss-of-function mutations in the Notch pathway have been identified in patients with chronic myelomonocytic leukemia,

consistent with the possibility that the myeloid-differentiation commitment of HSCs is enhanced by lower Notch activity[49]. This suggests a possible role for inactivation of *Satb1* in stem cells and progenitor cells in the pathogenesis of leukemia. As Satb1 is important for the epithelial-mesenchymal transition, and a greater abundance of Satb1 has been found in epithelial tumors[17,50], it will be of interest to determine whether Satb1, similar to its function in hematopoietic stem cells, modulates cell polarity and self-renewal in tumor stem cells and may thereby offer new opportunities for targeted therapy. In summary, our study has demonstrated that Satb1 critically modulated HSC fate 'decisions' by acting as a regulator of several functionally linked HSC properties. Our data showed that Satb1 was crucial for sustained HSC self-renewal by simultaneously governing gene networks that control cell fate, promoting quiescence and repressing lineage commitment in HSCs.

METHODS
Methods and any associated references are available in the online version of the paper.

Accession codes. GEO: microarray data, GSE44107; ERRBS data, GSE44304.

Note: Supplementary information is available in the online version of the paper.

1. Till, J.E. & McCulloch, E.A. A direct measurement of the radiation sensitivity of normal mouse bone marrow cells. *Radiat. Res.* **175**, 145–149 (1961).
2. Becker, A.J., McCulloch, E.A. & Till, J.E. Cytological demonstration of the clonal nature of spleen colonies derived from transplanted mouse marrow cells. *Nature* **197**, 452–454 (1963).
3. Spangrude, G.J., Heimfeld, S. & Weissman, I.L. Purification and characterization of mouse hematopoietic stem cells. *Science* **241**, 58–62 (1988).
4. Seita, J. & Weissman, I.L. Hematopoietic stem cell: self-renewal versus differentiation. *Wiley Interdiscip. Rev. Syst. Biol. Med.* **2**, 640–653 (2010).
5. Zeng, H., Yucel, R., Kosan, C., Klein-Hitpass, L. & Moroy, T. Transcription factor Gfi1 regulates self-renewal and engraftment of hematopoietic stem cells. *EMBO J.* **23**, 4116–4125 (2004).
6. Perry, J.M. & Li, L. Self-renewal versus transformation: Fbxw7 deletion leads to stem cell activation and leukemogenesis. *Genes Dev.* **22**, 1107–1109 (2008).
7. Antonchuk, J., Sauvageau, G. & Humphries, R.K. HOXB4-induced expansion of adult hematopoietic stem cells *ex vivo*. *Cell* **109**, 39–45 (2002).
8. Chang, K.C. *et al.* Interplay between the transcription factor Zif and aPKC regulates neuroblast polarity and self-renewal. *Dev. Cell* **19**, 778–785 (2010).
9. Scheel, C. *et al.* Paracrine and autocrine signals induce and maintain mesenchymal and stem cell states in the breast. *Cell* **145**, 926–940 (2011).
10. Bröske, A.M. *et al.* DNA methylation protects hematopoietic stem cell multipotency from myeloerythroid restriction. *Nat. Genet.* **41**, 1207–1215 (2009).
11. Sun, Y., Hu, J., Zhou, L., Pollard, S.M. & Smith, A. Interplay between FGF2 and BMP controls the self-renewal, dormancy and differentiation of rat neural stem cells. *J. Cell Sci.* **124**, 1867–1877 (2011).
12. Alvarez, J.D. *et al.* The MAR-binding protein SATB1 orchestrates temporal and spatial expression of multiple genes during T-cell development. *Genes Dev.* **14**, 521–535 (2000).
13. Yasui, D., Miyano, M., Cai, S., Varga-Weisz, P. & Kohwi-Shigematsu, T. SATB1 targets chromatin remodelling to regulate genes over long distances. *Nature* **419**, 641–645 (2002).
14. Beyer, M. *et al.* Repression of the genome organizer SATB1 in regulatory T cells is required for suppressive function and inhibition of effector differentiation. *Nat. Immunol.* **12**, 898–907 (2011).
15. Steidl, U. *et al.* A distal single nucleotide polymorphism alters long-range regulation of the PU.1 gene in acute myeloid leukemia. *J. Clin. Invest.* **117**, 2611–2620 (2007).
16. Savarese, F. *et al.* Satb1 and Satb2 regulate embryonic stem cell differentiation and Nanog expression. *Genes Dev.* **23**, 2625–2638 (2009).
17. Han, H.J., Russo, J., Kohwi, Y. & Kohwi-Shigematsu, T. SATB1 reprogrammes gene expression to promote breast tumour growth and metastasis. *Nature* **452**, 187–193 (2008).
18. Lakshminarayana Reddy, C.N., Vyjayanti, V.N., Notani, D., Galande, S. & Kotamraju, S. Down-regulation of the global regulator SATB1 by statins in COLO205 colon cancer cells. *Mol. Med. Rep.* **3**, 857–861 (2010).
19. Selinger, C.I. *et al.* Loss of special AT-rich binding protein 1 expression is a marker of poor survival in lung cancer. *J. Thorac. Oncol.* **6**, 1179–1189 (2011).
20. Cai, S., Han, H.J. & Kohwi-Shigematsu, T. Tissue-specific nuclear architecture and gene expression regulated by SATB1. *Nat. Genet.* **34**, 42–51 (2003).
21. Cai, S., Lee, C.C. & Kohwi-Shigematsu, T. SATB1 packages densely looped, transcriptionally active chromatin for coordinated expression of cytokine genes. *Nat. Genet.* **38**, 1278–1288 (2006).
22. Challen, G.A., Boles, N., Lin, K.K. & Goodell, M.A. Mouse hematopoietic stem cell identification and analysis. *Cytometry A* **75**, 14–24 (2009).
23. Matsumoto, A. *et al.* P57 is Required for Quiescence and Maintenance of Adult Hematopoietic Stem Cells. *Cell Stem Cell* **9**, 262–271 (2011).
24. Passegué, E., Wagers, A.J., Giuriato, S., Anderson, W.C. & Weissman, I.L. Global analysis of proliferation and cell cycle gene expression in the regulation of hematopoietic stem and progenitor cell fates. *J. Exp. Med.* **202**, 1599–1611 (2005).
25. Takizawa, H., Regoes, R.R., Boddupalli, C.S., Bonhoeffer, S. & Manz, M.G. Dynamic variation in cycling of hematopoietic stem cells in steady state and inflammation. *J. Exp. Med.* **208**, 273–284 (2011).
26. Wilson, A. *et al.* Hematopoietic stem cells reversibly switch from dormancy to self-renewal during homeostasis and repair. *Cell* **135**, 1118–1129 (2008).
27. Morita, Y., Ema, H. & Nakauchi, H. Heterogeneity and hierarchy within the most primitive hematopoietic stem cell compartment. *J. Exp. Med.* **207**, 1173–1182 (2010).
28. Kharas, M.G. *et al.* Musashi-2 regulates normal hematopoiesis and promotes aggressive myeloid leukemia. *Nat. Med.* **16**, 903–908 (2010).
29. Wu, M. *et al.* Imaging hematopoietic precursor division in real time. *Cell Stem Cell* **1**, 541–554 (2007).
30. Rhyu, M.S., Jan, L.Y. & Jan, Y.N. Asymmetric distribution of numb protein during division of the sensory organ precursor cell confers distinct fates to daughter cells. *Cell* **76**, 477–491 (1994).
31. Spana, E.P. & Doe, C.Q. Numb antagonizes Notch signaling to specify sibling neuron cell fates. *Neuron* **17**, 21–26 (1996).
32. Rebeiz, M., Miller, S.W. & Posakony, J.W. Notch regulates numb: integration of conditional and autonomous cell fate specification. *Development* **138**, 215–225 (2011).
33. Subramanian, A. *et al.* Gene set enrichment analysis: a knowledge-based approach for interpreting genome-wide expression profiles. *Proc. Natl. Acad. Sci. USA* **102**, 15545–15550 (2005).
34. Zeller, K.I. *et al.* Global mapping of c-Myc binding sites and target gene networks in human B cells. *Proc. Natl. Acad. Sci. USA* **103**, 17834–17839 (2006).
35. Huang, M.J., Cheng, Y.C., Liu, C.R., Lin, S. & Liu, H.E. A small-molecule c-Myc inhibitor, 10058–F4, induces cell-cycle arrest, apoptosis, and myeloid differentiation of human acute myeloid leukemia. *Exp. Hematol.* **34**, 1480–1489 (2006).
36. Delmore, J.E. *et al.* BET bromodomain inhibition as a therapeutic strategy to target c-Myc. *Cell* **146**, 904–917 (2011).
37. Pinto do, O.P., Kolterud, A. & Carlsson, L. Expression of the LIM-homeobox gene LH2 generates immortalized steel factor-dependent multipotent hematopoietic precursors. *EMBO J.* **17**, 5744–5756 (1998).
38. Mahmoudi, T. *et al.* The kinase TNIK is an essential activator of Wnt target genes. *EMBO J.* **28**, 3329–3340 (2009).
39. Fazzio, T.G., Huff, J.T. & Panning, B. An RNAi screen of chromatin proteins identifies Tip60-p400 as a regulator of embryonic stem cell identity. *Cell* **134**, 162–174 (2008).

40. Miyazaki, M. *et al.* The opposing roles of the transcription factor E2A and its antagonist Id3 that orchestrate and enforce the naive fate of T cells. *Nat. Immunol.* **12**, 992–1001 (2011).

41. Wontakal, S.N. *et al.* A large gene network in immature erythroid cells is controlled by the myeloid and B cell transcriptional regulator PU.1. *PLoS Genet.* **7**, e1001392.1–15 (2011).

42. Nerlov, C. & Graf, T.P.U. 1 induces myeloid lineage commitment in multipotent hematopoietic progenitors. *Genes Dev.* **12**, 2403–2412 (1998).

43. Orford, K.W. & Scadden, D.T. Deconstructing stem cell self-renewal: genetic insights into cell-cycle regulation. *Nat. Rev. Genet.* **9**, 115–128 (2008).

44. Cheng, T. *et al.* Hematopoietic stem cell quiescence maintained by p21cip1/waf1. *Science* **287**, 1804–1808 (2000).

45. Massagué, J. G1 cell-cycle control and cancer. *Nature* **432**, 298–306 (2004).

46. Xi, R. & Xie, T. Stem cell self-renewal controlled by chromatin remodeling factors. *Science* **310**, 1487–1489 (2005).

47. Reavie, L. *et al.* Regulation of hematopoietic stem cell differentiation by a single ubiquitin ligase-substrate complex. *Nat. Immunol.* **11**, 207–215 (2010).

48. Santaguida, M. *et al.* JunB protects against myeloid malignancies by limiting hematopoietic stem cell proliferation and differentiation without affecting self-renewal. *Cancer Cell* **15**, 341–352 (2009).

49. Klinakis, A. *et al.* A novel tumour-suppressor function for the Notch pathway in myeloid leukaemia. *Nature* **473**, 230–233 (2011).

50. Li, Q.Q. *et al.* Overexpression and involvement of special AT-rich sequence binding protein 1 in multidrug resistance in human breast carcinoma cells. *Cancer Sci.* **101**, 80–86 (2010).

ONLINE METHODS

Mice. *Satb1*^{−/−} mice[12] were provided by T. Kohwi-Shigematsu. C57BL/6 SJL CD45.1[+] mice were from Jackson Labs. All experimental procedures were approved by the Albert Einstein College of Medicine Institutional Animal Care and Use Committee (protocol 2011-0102).

Purification of hematopoietic stem and progenitor cells. Bone marrow cells were isolated from tibiae, femurs and pelvic bones. Fetal liver cells were isolated from embryos at E17–18.5. Lysis of red blood cells was followed by negative enrichment with Dynabeads (Invitrogen) with the following primary antibodies (all conjugated to phycoerythrin-indodicarbocyanine-Tricolor): anti-CD4 (GK1.5), anti-CD8a (53-6.7) and anti-CD19 (eBio1D3; all 1:100 dilution in PBS-FBS; all from eBioscience); and anti-B220 (RA3-6B2) and anti-Gr-1 (RB6-8C5; both 1:50 dilution; both from Invitrogen). Washed, unbound cells were stained with the following antibodies (all at a dilution of 1:30): allophycocyanin–Alexa Fluor 750–anti-CD117 (ACK2; eBioscience), Pacific blue–anti-Sca-1 (D7; Biolegend), fluorescein isothioyanate–anti-CD34 (RAM34; eBioscience), phycoerythrin-indodicarbocyanine–anti-CD16/32 (93; eBioscience), phycoerythrin–anti-CD150 (TC15-12F12.2; Biolegend) and allophycocyanin–anti-CD48 (HM48-1; Biolegend). Cells were sorted with a five-laser FACSAria II Special Order System flow cytometer (Becton Dickinson). Purity of sorted HSCs and MPPs was >98% for all experiments. Flow cyomtetyr data were analzyed with BD FACSDiva (Becton Dickinson) and FlowJo (TreeStar) software.

Colony formation and serial replating assays. Fetal liver cells or donor-derived adult stem and progenitor cells were plated (in technical duplicates) in MethoCult GF M3434 according to the manufacturer's recommendation (Stem Cell Technologies). Colonies were assigned scores after 7–10 d with an AXIOVERT 200M microscope (Zeiss).

RNA purification, real-time PCR and microarray. RNA was extracted with an RNeasy Micro kit (Qiagen), and quantity and quality were assessed with an Agilent 2100 Bioanalyzer (Agilent Technologies). For real-time RT-PCR, RNA was reverse-transcribed with Superscript II reverse transcriptase (Invitrogen) and was amplified (in technical triplicates) with specific primers (**Supplementary Table 5**) and the universal PCR Power SYBR Green mix (Applied Biosystems) on an iQ5 real-time PCR detection system according to the manufacturer's recommendation (Bio-Rad). For microarray studies, RNA was amplified with the WT Ovation Pico RNA amplification system (Nugen). After labeling with the GeneChip WT terminal labeling kit (Affymetrix), labeled cRNA was hybridized to Mouse Gene ST 1.0 microarrays (Affymetrix), stained and scanned by GeneChip Scanner 3000 7G system (Affymetrix) according to standard protocols.

HSC activation with 5-fluorouracil. C57BL/6 wild-type mice 4–8 weeks of age were injected intraperitoneally with 5-fluorouracil (150 mg per kg body weight; Sigma-Aldrich). After 0–12 d, CD150^{+}CD48^{−} LSK and CD150^{+}CD48^{+} LSK cells were isolated from the bone marrow by flow cytometry.

Analysis of microarray data. Raw data were normalized by the RMA algorithm of Affymetrix Power Tools (version 1.178). Probes with a median expression difference of >1.1-fold were considered to have a difference in expression, and probes with an s0 value of 5% as a cutoff for significance were considered to have a difference in expression by Significance Analysis for Microarrays in Multiple Experiment Viewer (version 4.8)[51]. After removal of unannotated and sex-specific genes that varied among the control samples, genes were clustered by hierarchical clustering, with optimization of sample and gene-leaf order, by Euclidean distance, complete linkage clustering. Gene-set enrichment analysis was done with all gene sets from the Molecular Signatures Database (version 3.0) and from the signature database of the Staudt laboratory (http://lymphochip.nih.gov/signaturedb).

Immunohistochemistry. Sorted cells were cytospun on poly-lysine-coated glass slides and dried and then were fixed with 4% paraformaldehyde and stained and then imaged on a Leica SP5 confocal microscope (Leica). Satb1 or Numb was detected with anti-Satb1 (1:250 dilution; EPR3895; Epitomics) or anti-Numb (1:100 dilution; ab14140; Abcam) according to the manufacturer's recommendation.

Reconstitution and competitive serial and limiting-dilution transplantation. Nucleated cells (1×10^6) from CD45.2[+] fetal livers were transplanted into lethally irradiated 6- to 8-week-old C57BL/6 SJL recipient mice by retro-orbital injection after total-body irradiation (950 cGy) with a Shepherd 6810 ^{137}Cs irradiator.

For serial transplantation assays, nucleated CD45.2^{+} donor cells (5×10^5), CD150^{+}CD11b^{+}Sca-1^{+}Lin^{−} fetal liver cells (5×10^1) or adult CD45.2^{+}CD150^{+} LSK cells (5×10^1) were transplanted along with CD45.1^{+} or CD45.1^{+}CD45.2^{+} total bone marrow competitor cells (5×10^5) into lethally irradiated C57BL/6 SJL mice. After 16–24 weeks, donor-cell chimerism and multilineage reconstitution were assessed, and CD45.2^{+} donor cells were isolated from the bone marrow of recipient mice by flow cytometry. Sorted CD45.2^{+} donor cells (5×10^5) were transplanted along with fresh CD45.1[+] or CD45.1[+]CD45.2[+] total bone marrow competitor cells (5×10^5) into the next cohort of lethally irradiated C57BL/6 SJL mice.

Limiting-dilution transplantation assays were done as described[52]. Reconstitution was monitored after 8–12 weeks and 16–24 weeks after transplantation. HSCs were quantified as competitive repopulating units with the L-Calc algorithm as described[53].

Analysis of cell-cycle activity in HSCs. Cell-cycle activity in HSCs was measured as incorporation of Hoechst 33342 and Pyronin Y as described[24]. Division kinetics of HSCs were determined by culture of sorted individual donor-derived wild-type or *Satb1*^{−/−} HSCs in CellGro media (CellGenix) with 50 ng/ml recombinant mouse stem-cell factor and 50 ng/ml recombinant mouse thrombopoietin. Deposition of individual cells in Terasaki plates was confirmed by microscopy 4 h after sorting. At 48 h after deposition, wells containing 1, 2 and >2 cells were counted by light microscopy.

HSC division-mode assay. For analysis of symmetric and asymmetric divisions, Numb distribution was monitored in HSCs undergoing division by immunohistochemistry as described[29].

Lineage tracing with the viability dye CMFDA. HSC commitment kinetics were monitored *in vivo* by a modified published protocol for lineage tracing with viability dyes[25]. CD45.2^{+}CD150^{+} LSK bone marrow cells from CD45.1^{+} recipient mice >20 weeks after transplantation were labeled with 2 μM CellTracker Green CMFDA (5-chloromethylfluorescein diacetate; Invitrogen). Labeled cells (5×10^3) were injected along with CD45.1[+] total bone marrow cells (5×10^5) into 6- to 8-week-old irradiated CD45.1[+] mice (450 rads). Labeled HSCs (5×10^2) were immediately analyzed by flow cytometry for incorporated CMFDA. At 4 d after transplantation, recipients were killed and nucleated bone marrow cells were stained with anti-CD45.2 (104; eBioscience), anti-CD150 (TC15-12F12.2; Biolegend), anti-c-Kit (ACK2; eBioscience), anti-Sca-1 (D7; Biolegend) and lineage markers. Cells were analyzed with the same flow cytometer setup and experimental protocol as used for the initial CMFDA-incorporation analysis. Gates for tracing of up to seven divisions were set as described[54].

ChIP. ChIP experiments were done as described[28]. Chromatin was isolated from mouse HPC7 cells and was sonicated with a Bioruptor (Diagenode). Immunoprecipitation was done with 5 μg anti-Satb1 (H-70; Santa Cruz Biotechnology) or 5 μg normal rabbit IgG (sc-2027; Santa Cruz Biotechnology). The Satb1-binding site SBS336 in the *Cd25* locus (encoding the α-chain of the receptor for interleukin 2) served as a positive control, and an intronic *Il2* site served as a negative control[13]. Binding of Satb1 to the *Myc* promoter was assessed with published primers[21].

ChIP of primary cells was done with the LowCell# ChIP kit (Diagenode). CD45.2^{+}CD150^{+} LSK cells were sorted from the bone marrow of a pool of recipients of *Satb1*^{−/−} or wild-type cells at >20 weeks after transplantation. Chromatin was isolated and then was sonicated with a Bioruptor sonicator. Immunoprecipitation was done with chromatin from 5×10^4 sorted cells and 2 μg of anti-H3K4me3 (GAH-8208), anti-H3K27me3 (GAH-9205)

or normal rabbit IgG (included in kits; all from Qiagen). Primers are in **Supplementary Table 6**.

Lentivirus-mediated restoration of Satb1. CD150+CD48– LSK cells were isolated from wild-type and *Satb1*–/– embryos at E17–18.5 and were infected with lentiviral particles expressing Satb1 or empty vector alone (pCAD-IRES-GFP) in Cellgro medium containing 50 ng/ml recombinant mouse stem-cell factor, 50 ng/ml recombinant mouse thrombopoietin and 8 μg/ml polybrene (Sigma) as described[15]. Viable, GFP+ cells were sorted by flow cytometry (cell purity, >98%; viability, >85%).

Numb knockdown. Wild-type or *Satb1*–/– CD45.2+CD150+CD48– LSK cells were isolated from recipient mice 16 and 20 weeks after transplantation and were transduced with lentiviral shRNA targeting mouse Numb or nontargeting control shRNA (Santa Cruz Biotechnology) by spin-infection. Supernatant was replaced with growth medium (CellGro containing 50 ng/ml recombinant mouse stem-cell factor and 50 ng/ml recombinant mouse thrombopoietin) after 4 h and HSCs were cultured for 32 h. Cells were plated in MethoCult GF M3434 containing 1 μg/ml puromycin (Sigma). Colonies were assigned scores and mRNA expression was measured 7–10 d after plating.

Inhibition of c-Myc. Wild-type and *Satb1*–/– CD45.2+CD150+CD48– LSK cells were isolated from recipient mice 16 and 20 weeks after transplantation. Cells were treated for 48 h with 10058-F4 (Santa Cruz Biotechnology) or JQ1 (provided by J. Bradner) in CellGro medium containing 50 ng/ml recombinant mouse stem-cell factor and 50 ng/ml recombinant mouse thrombopoietin. Pre-dilutions of each inhibitor (100×) were prepared in DMSO and added at a dilution of 1:100 to the culture medium of HSCs; 1% DMSO was added to mock-treated control cells. After 48 h of treatment, cells were plated in MethoCult GF M3434. Colonies were assigned scores after 7–10 d.

ERRBS. Sorted, *Satb1*–/– and wild-type CD45.2+CD150+ LSK cells, and wild-type CD45.2+CD150– LSK cells >20 weeks after transplantation were analyzed by ERRBS[55]. DNA (10 ng) was digested with MspI. End repair and ligation of paired-end Illumina sequencing adaptors was done, followed by size selection (150–400 base pairs) by gel extraction (Qiagen) and bisulfite treatment with the EZ DNA Methylation Kit (Zymo Research). PCR amplification with Illumina PCR PE1.0 and 2.0 primers was followed by isolation of library products with AMPure XP beads (Agencort). Quality control was achieved by quantification on a Qubit 2.0 fluorometer (Invitrogen) and library visualization with Quant-iT dsDNA HS Assay Kit (Agilent 2100 Bioanalyzer). Amplified libraries were sequenced with a 50–base pair single-end read run on a HiSeq2000 (Illumina). Image capture, analysis and base calling were done with CASAVA 1.8 (Illumina). After adaptor filtration with FAR software for the preprocessing of sequencing data (now called Flexbar; from sourceforge), bisulfite-converted 'reads' were aligned to the mm9 genome (http://genome.ucsc.edu/cgi-bin/hgGateway?db=mm9) with the bisulfite mapping tool Bismark[56], and methylation 'calls' were called on 'reads' with a Phred base-calling program quality score of >20 and ten- or fivefold coverage.

Analysis of ERRBS data. Methylation 'call' files were analyzed with methylKit (version 0.5.3)[57], a software package for DNA-methylation analysis and annotation from high-throughput bisulfite sequencing in the statistical programming language R/Bioconductor (version 2.15.2) with nonoverlapping DMRs 1 kb in length (10× coverage; >10% difference in methylation; q < 0.001). Differences in methylation were assessed in wild-type versus *Satb1*–/– CD150+ LSK cells and in wild-type CD150+ LSK cells versus wild-type CD150– LSK cells. DMRs were annotated for CpG islands, CpG shores (2 kilobases upstream and downstream from CpG islands) and isolated CpG, as well as RefSeq genes from mm9 with data provided by the UCSC Genome Browser. Promoters were considered to be 5 kilobases upstream of transcription start sites; regions farther than 5 kilobases upstream or downstream of RefSeq genes were considered intergenic. Region overlaps were determined with BEDTools, a flexible software suite of utilities for the comparison of genomic features[58]. Overlap of 'commitment DMRs' (wild-type HSCs versus wild-type MPPs) and '*Satb1*–/– HSC DMRs' (*Satb1*–/– HSCs versus wild-type HSCs) was determined by Bismark methylation 'calls' with a minimum coverage of five 'reads' per differently methylated cytosines (q < 0.001; >25% difference in methylation).

Statistical analysis. Statistical analysis of group comparisons was done with Student's *t*-test in Excel, GraphPad Prism. Statistical enrichment analysis was done with hypergeometrical testing with software of the R project for statistical computing.

51. Kossenkov, A.V. & Ochs, M.F. Matrix factorization for recovery of biological processes from microarray data. *Methods Enzymol.* **467**, 59–77 (2009).
52. Maggio-Price, L., Wolf, N.S., Priestley, G.V., Pietrzyk, M.E. & Bernstein, S.E. Evaluation of stem cell reserve using serial bone marrow transplantation and competitive repopulation in a murine model of chronic hemolytic anemia. *Exp. Hematol.* **16**, 653–659 (1988).
53. Szilvassy, S.J., Nicolini, F.E., Eaves, C.J. & Miller, C.L. Quantitation of murine and human hematopoietic stem cells by limiting-dilution analysis in competitively repopulated hosts. *Methods Mol. Med.* **63**, 167–187 (2002).
54. Lyons, A.B. Analysing cell division *in vivo* and *in vitro* using flow cytometric measurement of CFSE dye dilution. *J. Immunol. Methods* **243**, 147–154 (2000).
55. Akalin, A. *et al.* Base-pair resolution DNA methylation sequencing reveals profoundly divergent epigenetic landscapes in acute myeloid leukemia. *PLoS Genet.* **8**, e1002781 (2012).
56. Krueger, F. & Andrews, S.R. Bismark: a flexible aligner and methylation caller for Bisulfite-Seq applications. *Bioinformatics* **27**, 1571–1572 (2011).
57. Akalin, A. *et al.* methylKit: a comprehensive R package for the analysis of genome-wide DNA methylation profiles. *Genome Biol.* **13**, R87 (2012).
58. Quinlan, A.R. & Hall, I.M. BEDTools: a flexible suite of utilities for comparing genomic features. *Bioinformatics* **26**, 841–842 (2010).